One-dimensional germanium nanostructures—formation and their electron field emission properties

2010 Nanotechnology 21 455601

(http://iopscience.iop.org/0957-4484/21/45/455601)

Nanotechnology **21** (2010) 455601 (5pp) doi:10.1088/0957-4484/21/45/455601

One-dimensional germanium nanostructures—formation and their electron field emission properties

Hung-Chi Wu[1], Te-Chien Hou[1], Yu-Lun Chueh[1], Lih-Juann Chen[1], Hsin-Tien Chiu[2] and Chi-Young Lee[1,3]

[1] Department of Materials Science and Engineering, National Tsing Hua University, Hsinchu, 30013, Taiwan, Republic of China
[2] Department of Applied Chemistry, National Chiao Tung University, Hsinchu, 30010, Taiwan, Republic of China
[3] Center for Nanotechnology, Materials Science, and Microsystems, National Tsing Hua University, Hsinchu, 30013, Taiwan, Republic of China

E-mail: cylee@mx.nthu.edu.tw

Received 10 August 2010
Published 14 October 2010
Online at stacks.iop.org/Nano/21/455601

Abstract
Ge nanostructures were synthesized by reduction of GeO_2 in H_2 atmosphere at various temperatures. Entangled and straight Ge nanowires with oxide shells were grown at high temperatures. Ge nanowires with various numbers of nodules were obtained at low temperatures. Ge nanowires without nodules exhibited remarkable field emission properties with a turn-on field of 4.6 V μm^{-1} and field enhancement factor of 1242.

S Online supplementary data available from stacks.iop.org/Nano/21/455601/mmedia

(Some figures in this article are in colour only in the electronic version)

One-dimensional (1D) group IV nanostructures (NSs) have been extensively studied as functional components in electronic and optical systems. They may be used in the fabrication of fundamental nanodevices [1–12]. Therefore, the fabrication of group IV NSs has attracted much attention. Carbon nanotubes (CNTs) have generated considerable interest because of their unique properties and potential applications [1–4]. Silicon (Si), an abundant element in the earth, has also attracted substantial attention because of its important fundamental physical properties. Applications of Si nanowires (NWs) have been demonstrated in many micro- and nanodevices [5–9]. Recently, Ge has drawn much attention for its potential use in electronic and optoelectronic applications [10–12] because it has larger excitonic Bohr radius and higher electron and hole mobility than Si [13–15].

1D nanostructured materials are regarded as ideal electric field emission (EFE) sources because of their high aspect ratios. Many 1D materials, including CNTs [2], SiNWs [5], germanium (Ge) NWs [12], zinc oxide NWs [16], and tungsten oxide NWs [17], are regarded as highly promising candidates for field emitters. 1D GeNSs, such as NWs [10–12], nanorods [18], nanocones [19], and nanotubes [20] have been grown by vapor–liquid–solid (VLS) [11, 21, 22], vapor–solid (VS) [23], vapor–solid–solid [24], solution–liquid–solid [25], template-assisted growth [26], and oxide-assisted growth (OAG) routes [27]. A summary of synthesis methods for some GeNSs is listed in table S1 (available at stacks.iop.org/Nano/21/455601/mmedia). Among these approaches, the metal-catalyzed chemical vapor deposition (CVD) method is commonly adopted to grow NSs. However, the presence of catalytic-metal particles in NSs detrimentally affects the performance of electronic devices [28]. Therefore, non-catalytic growth of NSs has attracted substantial interest [23, 29].

In this work, GeNSs were synthesized by reduction of germanium (IV) oxide (GeO_2) powder in a H_2 atmosphere in a tube furnace at various deposition temperatures. A Si wafer was used as the substrate. The highly pure GeO_2 powder was placed in an alumina boat in the high temperature zone while the substrates were placed in the low temperature zone, downstream of the reaction chamber. The reacting gas, H_2, was introduced into the reaction chamber at a flow rate of

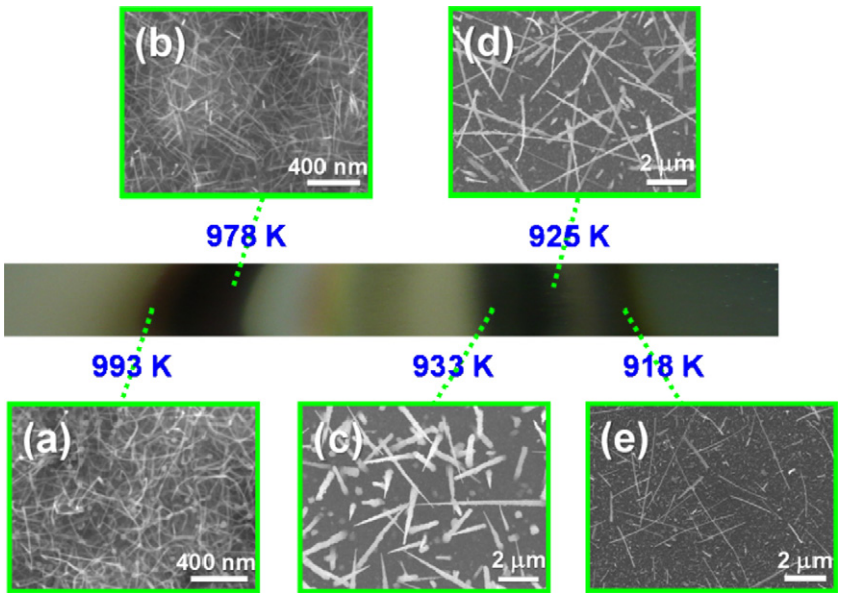

Figure 1. Optical micrographs of an as-synthesized specimen grown on a silicon substrate; (a)–(e) the corresponding temperatures and SEM images of the as-synthesized nanostructures in different regions.

65 sccm. The temperature of the high temperature zone was set to 1373 K with chamber pressure maintained at about 10 Torr and the reaction time was 6 h. A detailed experimental section and characterizations are depicted in supporting information (available at stacks.iop.org/Nano/21/455601/mmedia).

The as-synthesized specimen shows various colored regions. The colors and appearances of the different areas on the specimen vary with temperature (figure 1). The corresponding growth temperatures were about 1000–900 K. Based on x-ray diffraction (XRD) analysis and Raman study, these regions are all identified as crystalline Ge (figure S1 available at stacks.iop.org/Nano/21/455601/mmedia). From the scanning electron microscopy (SEM) images (figures 1(a)–(e)), different NSs had grown on a film above the substrate. Transmission electron microscopy (TEM)/energy dispersive spectroscopy (EDS) analysis indicated that the crystalline film is comprised of Ge only (figure S2 available at stacks.iop.org/Nano/21/455601/mmedia).

The SEM image of the specimen obtained at 993 K presents many entangled GeNWs with a drop-like end, which are designated as GeNS-A, which completely covered the Ge film over the substrate (figure 1(a)). The diameters of the individual NWs corresponding to the size of the end drop are in the range of 10–50 nm, while their lengths are of a few micrometers. The TEM and high-resolution TEM (HRTEM) images (figures 2(a), S3a and S3b available at stacks.iop.org/Nano/21/455601/mmedia) show that the drop-like end and the NW have a crystalline Ge core (about 7 nm in diameter), covered by a thick amorphous shell (with a thickness about 5–6 nm). According to the fast Fourier transform (FFT), GeNS-A has a preferential $[1\bar{1}0]$ orientation with a [111] zone axis (inset in figure S3b available at stacks.iop.org/Nano/21/455601/mmedia). The SEM image of the specimen obtained at 978 K shows many straight GeNWs, which are randomly grown on the substrate with diameters in the range of 10–50 nm and

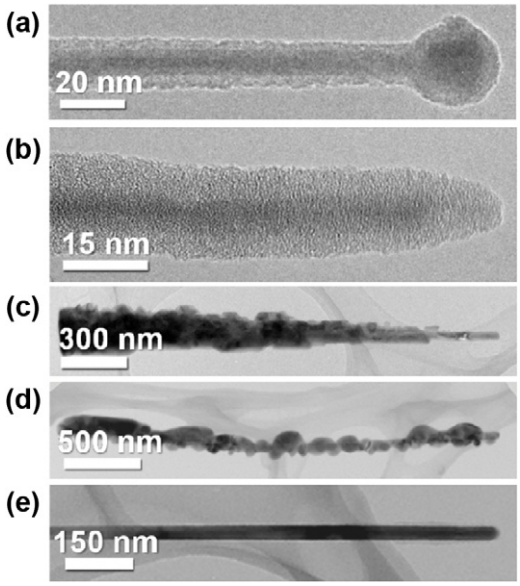

Figure 2. (a)–(e) TEM images of Ge nanostructures A–E, respectively.

lengths in the range of 100–400 nm, respectively. An example is shown in figure 1(b), for which these straight GeNWs are called GeNS-B. As presented in the TEM and HRTEM images (figures 2(b) and S3c available at stacks.iop.org/Nano/21/455601/mmedia), the NW has a crystalline Ge core with a diameter of 6 nm, having a preferential orientation in the [110] direction, and is surrounded by an amorphous shell 4–6 nm thick.

Taper-like wires with rough, scraggly and coarse surfaces grow randomly on the substrate at 933 K (figures 1(c), 2(c), and S4a available at stacks.iop.org/Nano/21/455601/mmedia), and are designated GeNS-C. GeNS-C are 3–15 μm long,

Table 1. The summary of growth conditions for GeNSs by reduction of GeO_2, and their EFE properties.

Sample	Growth temperature (K)	Morphology	Possible growth pathway	EFE	
				Turn-on field (V μm^{-1})	β
GeNS-A	993	Entangled wire	Self-catalytic VLS + OAG	—[a]	—[a]
GeNS-B	978	Wire	OAG	—[a]	—[a]
GeNS-C	933	Tapered-wire	VS + OAG	9.6	570
GeNS-D	925	Needle-wire	VS + OAG	5.8	825
GeNS-E	918	Wire	VS + OAG	4.6	1242

[a] Cannot be obtained.

with tip diameters of 30–200 nm and base diameters of 150–600 nm, respectively. The corresponding selected area electron diffraction (SAED) presents a spot pattern which is indexed as the [111] zone axis of crystalline Ge (figure S5a available at stacks.iop.org/Nano/21/455601/mmedia), revealing a preferential [11$\bar{2}$] orientation of the wire. The specimen that was deposited at 925 K comprises massive needle-like GeNWs with many protruding nodules, designated GeNS-D (figures 1(d) and S4b available at stacks.iop.org/Nano/21/455601/mmedia). GeNS-D are 3–15 μm long; the tip diameters are 50–100 nm, and the base diameters are 150–400 nm, that was also confirmed by the TEM image (figure 2(d)). The nodules are 50–500 nm long, with diameters of 10–100 nm, comprised only of Ge. The corresponding SAED patterns (figure S5b available at stacks.iop.org/Nano/21/455601/mmedia) and the fringes in HRTEM (figure S6 available at stacks.iop.org/Nano/21/455601/mmedia, taken from the rectangular region) show that the central GeNW has a preferential [1$\bar{1}$0] orientation with a zone axis of [111]; the Ge nodule has a zone axis of [110]. GeNWs with lengths of 0.5–10 μm and tip diameters of 20–120 nm were deposited at 918 K (figures 1(e), 2(e) and S4c available at stacks.iop.org/Nano/21/455601/mmedia); they are straight and uniform with smooth surfaces designated as GeNS-E. The SAED pattern (figure S5c available at stacks.iop.org/Nano/21/455601/mmedia) of the tip of the GeNS-E indicates that GeNS-E has a preferential [11$\bar{2}$] orientation with a zone axis of [111]. Further, HRTEM images (figures S7a, S7b and S7c available at stacks.iop.org/Nano/21/455601/mmedia) show that GeNS-C, GeNS-D, and GeNS-E have structure defects and amorphous shells of about 1–7 nm in size.

Based on the above observations, 1D diversiform GeNSs, such as entangled wires with droplet tips and oxide shells, straight wires with thick oxide shells, tapered wires with many nodules on their surfaces, needle-shaped wires with some nodules on their surfaces, and straight wires without nodules, were obtained in various regions of the substrates. This work presents a possible mechanism of formation of the various GeNSs as shown in figure 3. In high temperature regions, GeO_2 powder reacted with H_2 to form reactive species, GeO_x ($0 \leqq x < 2$), which are responsible for the deposition of Ge films. Substrate temperatures, chemical compositions and concentrations of reactive species seriously affect the formation of various GeNSs. Generally, wires obtained in the high temperature region by the VLS route appear with

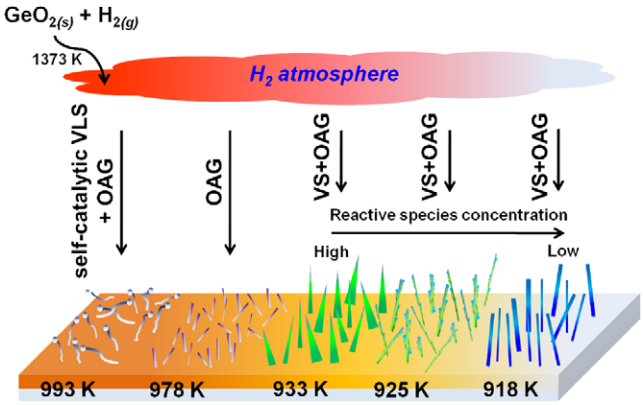

Figure 3. Proposed pathways of the growth of various Ge nanostructures.

a catalyst particle on the tip due to the formation of liquid droplets as a catalyst. VS products are typically obtained in the low temperature areas [27]. While oxide species were used as precursors, wires with a crystalline core in an oxide sheath are typical OAG products [27]. Owing to the different freezing points of GeO_x, the oxygen-rich GeO_x might be the precursors at the high temperature upstream region, while oxygen-poor species were the precursors in the low temperature downstream region. Additionally, the concentration of reactive species is higher in the upstream region, so thick wires or many wires are formed, while in the downstream region, the lower concentration of reactive species causes thin wires or few wires to be formed.

The appearance, synthesis, and the proposed formation of the GeNSs are summarized in table 1. In the upstream region, oxygen-rich GeO_x species are the major precursors, Ge wires with a thick amorphous oxide shell and spheroid end were obtained at 993 K (TEM images of this wire are shown in figures 2(a), S3a and S3b available at stacks.iop.org/Nano/21/455601/mmedia). The spheroid end wires are typical self-catalytic VLS products [30]. The crystalline wires with an amorphous oxide shell are typical OAG products. Accordingly, the formation of GeNS-A was proposed by a combined VLS and OAG route. GeNS-B with a thick amorphous oxide shell obtained at 978 K is a representative OAG product. Crystalline germanium nanostructures (GeNS-C, GeNS-D and GeNS-E) with structure defects inside covered by a thin sheath of amorphous shell were obtained in the downstream region (940–910 K), where oxide-poor GeO_x were the major

precursors. Thus, it is suggested that GeNS-C, GeNS-D, and GeNS-E are oxide-assisted VS products with a diminished thickness of the amorphous oxide shell. In such regions, 1D nanomaterials with various dimensions and different numbers of nodules growing were obtained [31]. In the front part of this region, where the concentration of reactive species exceeded that in the hind region, wider wires with more nodules caused by side growth were observed. As described in the preceding paragraph, the average diameters of GeNS-C, GeNS-D, and GeNS-E declined from approximately 450 nm to 200 nm, and to 60 nm, respectively.

The EFE properties of GeNS-C, GeNS-D, and GeNS-E are summarized in table 1. Figure 4(a) plots the field emission current density against the applied electric field (J–E) and the corresponding Fowler–Nordheim (FN) plot [32]. Notably, the turn-on field was estimated from the FN plot of the J–E curve by finding the intersection of two straight lines that were extrapolated from the low-field and high-field sections of the FN plot [33]. In such plots, these straight lines show that the emission currents satisfy the following conventional FN equation:

$$J = (A\beta^2 E^2/\Phi)\exp(-B\Phi^{3/2}/\beta E),$$

where J is the current density in A m^{-2}; E is the electric field in V m^{-1}; Φ represents the work function in eV; β is the field enhancement factor at a sharp point of the material; $A = 1.54 \times 10^{-6}$ A eV V^{-2}, and $B = 6.83 \times 10^{9}$ eV$^{-3/2}$ V m^{-1}. β is given by $\beta = \Phi^{3/2}/\Phi_e$ using the reported value for $\Phi = 5.15$ eV for Ge, where Φ_e denotes the effective work function that is determined from the gradient of the FN plot. Since the tip morphologies of GeNS-C, D, and E are similar, the improvement of EFE properties might be caused by the diminishing of the oxide shell (as shown in figure S7 available at stacks.iop.org/Nano/21/455601/mmedia). The remarkable EFE properties of GeNS-E showed that the turn-on field and field enhancement factor were about 4.6 V μm^{-1} and 1242, respectively. In addition, the EFE stability measurement was performed by keeping the electric field at 10 V μm^{-1} on the GeNS-E. The emission current was recorded for 1000 s, as shown in the upper right inset of figure 4(a); in the entire measurement, the current remained steadily between 0.55 to 0.57 mA cm^{-2}. Further, the EFE properties of the GeNS-E were superior to several potential candidates for field emitters, and a rough comparison of the EFE properties of Ge, CNTs, Si, ZnO, and WO_3 nanowires are shown in table S2 (available at stacks.iop.org/Nano/21/455601/mmedia).

Figure 4(b) plots the I–V curve of a single GeNS-C and GeNS-E obtained by making two-terminal measurements. The insets present SEM images of GeNS-C and GeNS-E when their electrical transport properties are being measured. The I–V relationships are approximately linear, indicating favorable ohmic contacts of the GeNSs with electrodes. The average electrical resistivities of the single GeNS-C and GeNS-E are about 0.3 and 83 Ω cm obtained using about 20 wires, respectively.

In summary, germanium nanostructures were synthesized by reducing GeO_2 powder in a H_2 atmosphere. In high temperature regions of the substrates, entangled and straight Ge nanowires (GeNS-A and B) with an oxide shell with a thickness of about 5 nm and a diameter of 10–50 nm were obtained via self-catalytic VLS and OAG pathways. Freestanding Ge nanostructures that were tapered, needle-shaped, and wire-shaped (GeNS-C, D, and E) with various numbers of nodules were obtained in the low temperature area of the substrates obtained via an oxide-assisted VS pathway. The length of these structures was up to many micrometers, and their average diameters were about 450, 200, and 60 nm, respectively. Of these nanostructures, freestanding Ge nanowires without nodules (GeNS-E) exhibited remarkable EFE properties, with a turn-on field of 4.6 V μm^{-1} and a field enhancement factor of 1242. The resistivities of tapered and wire-shaped freestanding Ge nanostructures (GeNS-C and E) were 0.3 and 83 Ω cm, respectively. Such structures could be adopted in future electronic and optoelectronic nanodevices.

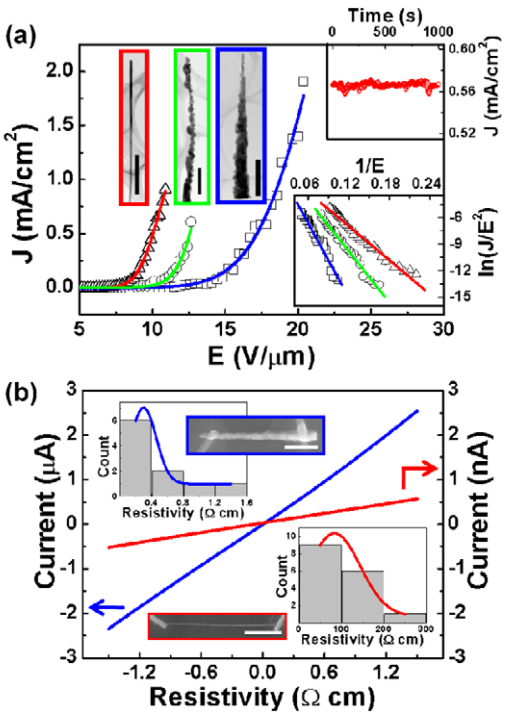

Figure 4. (a) The electron field emission properties and current density–field (J–E) plots of GeNS-C, D, and E; the upper left insets are the corresponding Ge nanostructure images (scale bar: 500 nm); the upper right inset shows the corresponding FN plots; the lower right inset shows the stability test of GeNS-E under 10 V μm^{-1}. (b) I–V curve of a single GeNS-C and GeNS-E obtained using a two-terminal I–V measurement; the inset shows corresponding SEM images of samples for I–V measurement, as well as their resistivity statistics (scale bar: 2 μm).

Acknowledgments

The authors would like to thank the National Science Council of the Republic of China, Taiwan, for financially supporting this research under contract No. NSC-96-2113-M-007-021.

References

[1] LeRoy B J, Lemay S G, Kong J and Dekker C 2004 *Nature* **432** 371

[2] Deheer W A, Chatelain A and Ugarte D 1995 *Science* **270** 1179
Rao A M, Jacques D, Haddon R C, Zhu W, Bower C and Jin S 2000 *Appl. Phys. Lett.* **76** 3813

[3] Bachtold A, Hadley P, Nakanishi T and Dekker C 2001 *Science* **294** 1317

[4] Rueckes T, Kim K, Joselevich E, Tseng G Y, Cheung C L and Lieber C M 2000 *Science* **289** 94

[5] Chueh Y L, Chou L J, Cheng S L, He J H, Wu W W and Chen L J 2005 *Appl. Phys. Lett.* **86** 133112

[6] Cui Y and Lieber C M 2001 *Science* **29** 851

[7] Ahn Y, Dunning J and Park J 2005 *Nano Lett.* **5** 1367

[8] Hayden O, Agarwal R and Lieber C M 2006 *Nat. Mater.* **5** 352

[9] Stern E, Klemic J F, Routenberg D A, Wyrembak P N, Turner-Evans D B, Hamilton A D, LaVan D A, Fahmy T M and Reed M A 2007 *Nature* **445** 519

[10] Andzane J, Petkov N, Livshits A I, Boland J J, Holmes J D and Erts D 2009 *Nano Lett.* **9** 1824

[11] Ahn Y H and Park J 2007 *Appl. Phys. Lett.* **91** 162102

[12] Li L, Fang X S, Chew H G, Zheng F, Liew T H, Xu X J, Zhang Y X, Pan S S, Li G H and Zhang L D 2008 *Adv. Funct. Mater.* **18** 1080

[13] Tu R, Zhang L, Nishi Y and Dai H J 2007 *Nano Lett.* **7** 1561

[14] Prasankumar R P, Choi S, Trugman S A, Picraux S T and Taylor A J 2008 *Nano Lett.* **8** 1619

[15] Sze S M 1981 *Physics of Semiconductor Devices* (New York: Wiley)

[16] Tseng Y K, Huang C J, Cheng H M, Lin I N, Liu K S and Chen I C 2003 *Adv. Funct. Mater.* **13** 811

[17] Chang M T, Chou L J, Chueh Y L, Lee Y C, Hsieh C H, Chen C D, Lan Y W and Chen L J 2007 *Small* **3** 658

[18] Mei Y F, Li Z M, Chu R M, Tang Z K, Siu G G, Fu R K Y, Chu P K, Wu W W and Cheah K W 2005 *Appl. Phys. Lett.* **86** 021111

[19] Jin C B, Yang J E and Jo M H 2006 *Appl. Phys. Lett.* **88** 193105

[20] Mei Y F, Siu G G, Li Z M, Fu R K Y, Tang Z K and Chu P K 2005 *J. Cryst. Growth* **285** 59

[21] Morales A M and Lieber C M 1998 *Science* **279** 208

[22] Sutter E, Ozturk B and Sutter P 2008 *Nanotechnology* **19** 435607

[23] Kim B S, Koo T W, Lee J H, Kim D S, Jung Y C, Hwang S W, Choi B L, Lee E K, Kim J M and Whang D 2009 *Nano Lett.* **9** 864

[24] Lensch-Falk J L, Hemesath E R, Perea D E and Lauhon L J 2009 *J. Mater. Chem.* **19** 849

[25] Chockla A M and Korgel B A 2009 *J. Mater. Chem.* **19** 996

[26] Al-Salman R, Mallet J, Molinari M, Fricoteaux P, Martineau F, Troyon M, El Abedin S Z and Endres F 2008 *Phys. Chem. Chem. Phys.* **10** 6233

[27] Peng H Y, Pan Z W, Xu L, Fan X H, Wang N, Lee C S and Lee S T 2001 *Adv. Mater.* **13** 317
Zhang R Q, Lifshitz Y and Lee S T 2003 *Adv. Mater.* **15** 635
Wang N, Tang Y H, Zhang Y F, Lee C S and Lee S T 1998 *Phys. Rev.* B **58** 16024

[28] El Bouayadi R, Regula G, Pichaud B, Lancin M, Dubois C and Ntsoenzok E 2000 *Phys. Status Solidi* b **222** 319

[29] Ho S T, Chen K C, Chen H A, Lin H Y, Cheng C Y and Lin H N 2007 *Chem. Mater.* **19** 4083

[30] Gu Z J, Liu F, Howe J Y, Paranthaman M P and Pan Z W 2009 *Cryst. Growth Des.* **9** 35
Orlandi M O, Leite E R, Aguiar R, Bettini J and Longo E 2006 *J. Phys. Chem.* B **110** 6621
Chen Y Q, Cui X F, Zhang K, Pan D Y, Zhang S Y, Wang B and Hou J G 2003 *Chem. Phys. Lett.* **369** 16

[31] Chen X L, Li J Y, Lan Y C and Cao Y G 2001 *Mod. Phys. Lett.* B **15** 27

[32] Fowler R H and Nordheim L 1928 *Proc. R. Soc.* A **119** 173

[33] Tzeng Y F, Lee Y C, Lee C Y, Lin I N and Chiu H T 2007 *Appl. Phys. Lett.* **91** 063117
Wu H C, Tsai T Y, Chu F H, Tai N H, Lin H N, Chiu H T and Lee C Y 2010 *J. Phys. Chem.* C **114** 130